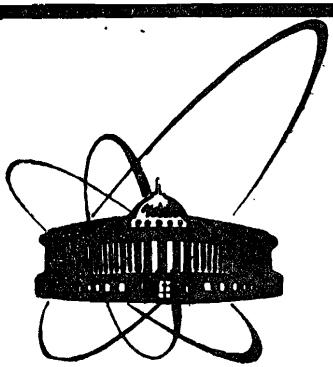

объединенный
институт
ядерных
исследований
дубна

E6-86-231

E.G.Nadjakov

ATOMIC BEAM COLLIMATION

Submitted to "Journal of Physics E:
Scientific Instruments"

1986

This problem is a rather old one: since the beginning of the century. We are going to consider it again in connection with the recently developed optical methods for nuclear moments determination via hyperfine structure measurements, based on dye laser spectrometers [1,2]. We aim practical conclusions about atomic flux and density distributions over space (section 2) and velocity (section 3) in order to apply them in the Dubna laser spectroscopy group work [3,4] for determination and prediction of laser spectrometer parameters. Methods to do it will be described in another publication [5]. We are going to mention one of the last and still rather old references on our present problem [6], and direct the reader to its references for older work, and a new publication [7], where this problem has been considered again with the same purpose as here, both experimentally and theoretically (see end of section 2). Our approach has succeeded moreover to offer: 1) simple analytical including integral formulae easy for applications (section 4); 2) validity under minimal limiting assumptions, the basic of them formulated in section 1, and thus also in extreme cases, like, e.g., laser ray very near to collimator (section 5); 3) simplicity in generalization beyond basic assumptions (section 6).

1. Basic assumptions

The essential geometrical situation is shown in fig. 1. The atomic beam oven is at the left-hand side, with a sample to be evaporated inside, kept at an absolute temperature T [K]. Our first assumption is that inside the oven the vapour pressure P [Pa] is

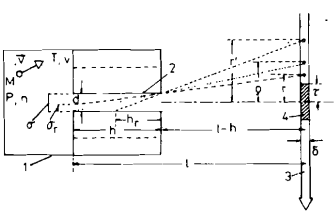

Fig.1. Set up scheme: 1. atomic oven; 2. beam collimator; 3. laser ray; 4. interaction region (shaded). Fluorescence light is collected in a perpendicular to the drawing direction by a lens system on a photomultiplier; interaction region length $2\tilde{r}$ along laser ray determined by the diameter of photocathode image via lens system on laser ray.

the saturated one obtained from empirical tables [8]. This may not be so if the sample and/or its surface are not pure. The possible hindrances like ideal solution laws and deviations from them due to diffusion inside the sample and/or to evaporation from the sample surface have been discussed in an experimental publication of our group [4]. From P and T one can deduce the vapour concentration in the oven n :

$$n = P/kT \tag{1}$$

assumed to be homogeneous in space $\vec{r}$, and according to Maxwell's law with respect to velocity $\vec{v}$ in the oven, with the most probable value:

$$v = \sqrt{2kT/M}, \tag{2}$$

where k is the Boltzmann constant; and M , the mass of the atom.

Next comes the collimator, supposed to be kept at the same temperature in order to scatter the atoms hitting his walls. We assume on the second place that vapour pressure is low enough, so that for the mean free path λ compared to the collimator length h , we have $\lambda \gg h$. On the third place we suppose that diffuse scattering of atoms from collimator walls according to the cosine law takes place. Quantitatively, if we denote by μ the ratio of scattering to reflection plus scattering coefficients, then $\mu \approx 1$. Also $n = n(h_r)$ is linearly decreasing along the collimator [6]. Selfconsistency requires that it decreases from n for $h_r = h$ to 0 for $h_r = 0$, and determines the collimator transmission.

The laser ray intersects the atomic beam in, and the fluorescence light produced is focused on the photocathode from the so-called interaction region with a cross section S perpendicular to the atomic beam axis and a volume V , as follows:

$$S = 2\tau\delta \qquad V = 2\tau \frac{\pi}{4} \delta^2 \tag{3}$$

to be compared with an infinite plane area S_∞ at $l \gg h$, d oriented in the same way, and with an infinite volume V_∞ with base S_∞ and thickness $\frac{\pi}{4}\delta$.

The interplay of the collimator diameter d with atomic beam diameter on the laser ray 2ϱ :

$$\varrho_+ = \varrho + d/2 = ld/h, \qquad \varrho_- = \varrho - d/2 = (l-h)d/h \tag{4}$$

(by analogy, for any letter an index + will mean addition; and index - , subtraction of d/2 , e.g., $d_+ = 3d/2$, $d_- = d/2$) and with photocathode image on the laser ray diameter 2τ , determines the notations:

$$\tau_0 = 0, \quad \tau_1 = \min(d_-, \tau), \quad \tau_2 = \min(\varrho, \tau), \quad \tau_3 = \min\left(\max(\varrho, 5d/2), \tau\right), \quad \tau_4 = \tau. \tag{5}$$

The following cross sections and volumes will be used too:

$$S_0 = \delta^2, \qquad V_0 = \frac{\pi}{4}\delta^3$$
$$S_i = 2\tau_i\delta, \qquad V_i = 2\tau_i \frac{\pi}{4}\delta^2; \quad i = 1, 2. \tag{6}$$

The geometrically seen collimator lenght h_r from a point at a distance r from the interaction region centre along the laser ray is:

$$h_r = \begin{cases} h, & 0 \le r \le \varrho \\ h\varrho_-/r_-, & \varrho \le r < \infty. \end{cases} \tag{7}$$

The real collimator cross section is σ , and the geometrically seen cross section σ_r from a point at a distance r for a square hole is:

$$\sigma_r = \begin{cases} \sigma, & 0 \le r \le d_- \\ \sigma(1 - r_-/\varrho_-), & d_- \le r \le \varrho \\ 0, & \varrho \le r < \infty \end{cases} \tag{8}$$

Under the above mentioned assumptions the ratio of atoms, scattered from collimator walls, to directly passed through collimator, on the laser ray at $r \approx \varrho/2$ is $\mathcal{K}$, where:

$$\mathcal{K} = \mathcal{K}_0 \varepsilon, \qquad \mathcal{K}_0 = 1/2, \qquad \varepsilon = l(l-h) = \varrho_+/\varrho_- \tag{9}$$

$\mathcal{K}_0 = 1/2$ for a square collimator hole (or $\mathcal{K}_0 = 2/\pi$ for a round hole).

2. Space distribution

Let us denote by $\eta^{(S)}(r)$ the number of atoms passing in unit time a unit area of a plane, containing the laser ray, perpendicular to the atomic beam axis, at a distance r from the interaction region centre (the flux); and by $\eta^{(V)}(r)$, the number of atoms in a unit volume at the same place (the density). We introduce the notations, necessary in the following:

$$\bar{\bar{x}} = \begin{cases} 0, & x \le 0 \\ x, & 0 \le x \end{cases} \qquad \|x\| = \begin{cases} x, & x \le 1 \\ x^{-1}, & 1 \le x \end{cases} \tag{10}$$

$$\bar{r} = \begin{cases} r, & 0 \le r \le d_- \\ \dfrac{\varrho r - d_-^2}{\varrho_-}, & d_- \le r \le \varrho \\ r_+, & \varrho \le r < \infty \end{cases} \tag{11}$$

valid also for r changed to τ_i,

$$\bar{\ell}_r = \ell \times \min\left[1,\ 3/(2\varepsilon),\ r_+/(\bar{\bar{r}}_- \varepsilon)\right]. \tag{12}$$

Also:

$$f(x) = 1 + x^2, \qquad g(x) = \operatorname{arc\,tg}(x) \tag{13}$$

$$\eta_o^{(S)} = \frac{2}{\sqrt{\pi}}\, n v \frac{\sigma}{4\pi \ell^2}, \qquad \eta_o^{(V)} = n \frac{\sigma}{4\pi \ell^2}$$
$$n_S = 2, \qquad n_V = 3/2. \tag{14}$$

With these notations both flux and density distributions become:

$$\eta^{(S,V)}(r) = \eta_o^{(S,V)} \left\{ \frac{\overline{\overline{1 - \bar{\bar{r}}_-/\varrho_-}}}{\left[f(\bar{r}/\ell)\right]^{n_{S,V}}} + \frac{\varkappa}{\varepsilon} \frac{\overline{\overline{-r_-/\varrho_-}}}{\left[f(r_-/\bar{\ell}_r)\right]^{n_{S,V}}} \right.$$
$$\left. + \varkappa \frac{\|r_+/\varrho_+\|}{\left[f(r_+/\bar{\ell}_r)\right]^{n_{S,V}}} + \varkappa \frac{d_-}{r_+} \frac{\|r_+/\varrho_+\|}{\left[f(\bar{r}/\bar{\ell}_r)^{n_{S,V}}\right]} \left[1 - \overline{\overline{(1 - \bar{\bar{r}}_-/\varrho_-)}}\right] \right\}. \tag{15}$$

Note that (15) and further formulae for velocity (20) and integral (Appendix) simplify if the collimator finite dimensions are neglected: $h \ll l$.

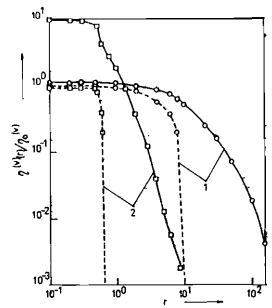

Fig.2. Space (r) distribution of atomic density (15) $\eta^{(V)}(r)$ in a normal case: $l = 100$, $h = 10$, $d = 1$, $\delta = 1$ (1, circles), and in a case of laser ray extremely near to collimator exit: $l = 11$, everything else the same (2, squares); all distances in mm. Both are presented with scattering from collimator $\varkappa \neq 0$ (solid lines) and without it $\varkappa = 0$ (dashed lines).

To get an impression about their behaviour, one of the space distributions is shown in fig. 2. As one can see, increasing l increases the linear broadening both with and without scattering from collimator walls. Scattering makes the distributions much broader in both cases presented. Without scattering they disappear at $\varrho \le r$ and are similar in angular units at $r < \varrho$. In the case of normal distance between collimator and laser ray, the density near to the atomic beam axis ($r \approx 0$) is changed insignificantly when scattering is included. In the opposite case of a laser ray extremely near to collimator exit differences appear. They are especially evident at $r \approx 0$: the density is significantly increased with and mostly due to scattering from collimator walls.

We take for comparison the experimental information for the angular distribution width at half height from fig. 14 of ref. /7/. In the cases $h/d = 13$ and $h/d = 7$ the experimental data are 4.7° and 8.1°. Theoretically by a Monte Carlo method in fig. 13 of ref. /7/, the same authors obtain 2.8° and 5.8°. Our calculation gives 4.8° and 8.6°. This means that the discrepancy between theory and experiment, mentioned by the authors of ref. /7/, is avoided here. The reason for the better agreement of the present re-

sults with experiment may be the fact that diffuse scattering is taken into account here. This phenomenon is suggested in ref. /7/ as the origin of their discrepancy.

3. Velocity distribution

In the normal case (see fig. 2) the distribution over the relative velocity u component along the laser ray to the one along the atomic beam axis is very near to that of the density $\eta^{(V)}(r)$ if $u = r_+/l$ for $r \leq \varrho$ and $u = r_-/(1-h)$ for $\varrho \leq r$. However, in the extreme case differences occur. Moreover, in connection with the relation of relative velocity u to shift $\Delta\nu$ of frequency ν (first order Doppler effect):

$$\Delta\nu = 2\sqrt{\ln 2}\ \frac{u_o}{\sqrt{f(u_o)}}\ \frac{v}{c}\ \nu\,, \tag{16}$$

where for the moment we can insert $u_o \longrightarrow u$ (for u_o : see section 4), the frequency shift distribution will be $\zeta(u)\,d\nu$ proportional to $[f(u)]^{n_V}\,\eta^{(V)}(u)d\nu$. This means that the denominator in (15) $[f(u)]^{n_V}$ will disappear in $\zeta(u)$: see (20). It will make the frequency distribution broader at high u.

Therefore we are going to obtain the relative velocity $\zeta(u)[f(u)]^{-n_V}du$ or the frequency $\zeta(u)d\nu$ distribution independently. First of all, the Maxwell velocity distribution has been approximately taken into account by the $\sqrt{\ln 2}$ coefficient in (16), where $2\sqrt{\ln 2} \approx 1.665$. Then the finite dimensions of the collimator have been considered approximately too. Let us introduce the additional notations:

$$\begin{aligned} v_o &= d/h = \varrho_+/l = \varrho_-/(l-h) \\ w_o &= 2d/(l-h) = 2(\varepsilon - 1)\,v_o \end{aligned} \tag{17}$$

$$\overline{\varkappa_u} = \varkappa \times \min\left[1,\ 3/(2\varepsilon),\ v_o/u,\ 3v_o/(2u + w_o)\right] \tag{18}$$

and

$$h(x) = \begin{cases} 1 - \varepsilon^{-1} + \frac{1}{2}(1+\varepsilon^{-1})\,x\,, & x \leq 1 \\ 1 + \frac{1}{2}\,\frac{\varepsilon - 1}{x + \varepsilon - 1}\,, & 1 \leq x\,. \end{cases} \tag{19}$$

Witn (10) and these notations, the numerator of the relative velocity, corresponding to the frequency distribution, becomes:

$$\zeta(u) = \zeta_o\left\{\overline{1 - u/v_o} + \overline{\varkappa_u}\ h(u/v_o)\right\}. \tag{20}$$

This distribution is shown in fig. 3 for the same cases as the space one in fig. 2. One can see that the normal case distributions in fig. 3 are similar to those in fig.2, except that the one with scattering

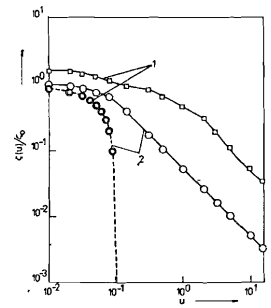

Fig.3. Frequency shift $\Delta\nu$ or numerator of relative velocity u distribution (20) $\zeta(u)$. The rest as for fig. 2.

becomes broader at high u, as espected above; without scattering both cases completely coincide, disappearing at $v_o \leq u$. In the case of extreme nearness a similar broadening with scatterig in fig. 3 compared to fig. 2 remains at high u. But at low u the behaviour is rather different: e.g., the significant rise of the curve with scattering as compared to that without it in fig. 2 becomes much lower in fig. 3.

4. Integral quantities and Doppler width

We introduce the integral flux of atoms Ψ through the infinite area S_∞, i.e., in all directions (total flux), and the integral number of atoms θ in the infinite volume V_∞ (total number):

$$\Psi = \int_{S_\infty} \eta^{(S)}\,dS\,, \qquad \theta = \int_{V_\infty} \eta^{(V)}\,dV\,. \tag{21}$$

We also introduce the integral flux of atoms φ through the interaction region cross section S (local flux) and the integral number of atoms χ in the interaction region volume V (local number):

$$\varphi = \int_S \eta^{(S)}\,dS\,, \qquad \chi = \int_V \eta^{(V)}\,dV\,. \tag{22}$$

Both integrations can be performed numerically by using the space distributions (15). However for the user it is preferable if simple analytical formulae could be obtained. Such formulae are given in the Appendix. The integration in (21) can be performed immediately. The integration in (22) contains approximations in order that the final formulae may become long, but remain simple to use. However care has been taken that the final formulae do not lose the quality of (15) to take into account the finite dimensions of the atomic beam collimator and laser ray. So they remain approximately valid even in the case of a laser ray extremely near to collimator exit.

The Doppler width in terms of relative velocity u is defined as full width at half maximum of the frequency distribution. Without taking the finite length of the interaction region for the moment into account, this definition gives the equation for u :

$$\zeta(u) = \frac{1}{2}\,\zeta(0). \qquad (23)$$

This equation can also be solved numerically by using the frequency distribution (20). But it is again preferable to obtain the solution analytically in a simple form, without losing the quality of (20) to take into account the finite dimensions of the atomic beam collimator. Such a formula for the solution u of (23) is given in the Appendix as well.

However, the finite length 2τ of the interaction region imposes an upper limit t on the active relative velocities u yielding corresponding frequency shifts $\Delta\nu$. This limit t is also found in the Appendix. Then the real frequency distribution will have the width (16), where

$$u_o = \min(u, t). \qquad (24)$$

5. Numerical results

Calculations of all the integral fluxes and numbers (21, 22) and of the Doppler widths (16), by using the Appendix, are shown in figs. 4 and 5. Let us note that Ψ/Ψ and χ/θ yield two definitions of the collimation efficiency, rather near to each other. Also the variations of the numbers θ and χ with changes of the parameters are rather near to those of the fluxes Ψ and Ψ respectively. Therefore only numbers and widths (but not fluxes) have been demonstrated in figs. 4 and 5. Due to the logarithmic vertical scale,

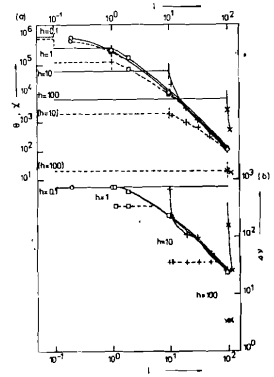

Fig. 4. (a) Total number of atoms (30) θ atom (horizontal lines at unreal $l \leq h$ can be prolonged to any real $l > h$ since θ does not depend of l), local number of atoms (38) with (31-37) χ atom (curved lines at real $l > h$), and (b) Doppler width (16) with (24, 39, 40) $\Delta\nu$ MHz (a horizontal line above is the maximal $\Delta\nu$ at the accepted v_s , ν). dependencies on distance of laser ray to collimator entrance l , for different collimator lengths: $h = 0.1$ (circles), $h = 1$ (squares), $h = 10$ (crosses), $h = 100$ (x's), at an atomic beam collimator diameter $d = 1$, a laser ray diameter $\delta = 1$, an interaction region length $2\tau = 6$; all distances in mm . With atomic scattering from collimator walls $\varkappa \neq 0$ (solid lines) and without it $\varkappa = 0$ (dashed lines). For "standard" n_s , v_s (see caption to the table).

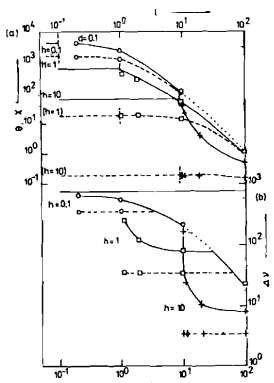

Fig. 5. The same as for fig. 4 except: collimator diameter $d = 0.1$ mm ; extrapolation (dotted lines).

the reciprocal collimation efficiency θ/χ is presented by the distance between the horizontal line for θ and curved line for χ , its limit for $l \to h$ being l (0 distance), as it should be.

From figs. 4 and 5 one can see the improvement of collimation efficiency χ/θ at shorter distances l/d and longer collimators h/d as expected. However one sees immediately that at real laser ray to collimator exit distances $l - h$ one can hardly expect an efficiency better than 1% . The numbers of atoms with scattering from collimator walls are higher than those without, and become almost the same at high distances $l \gg h$, but the efficiencies are lower and tend to 1 , becoming almost the same, at low distances $l \approx h$.

One observes an improvement in Doppler width $\Delta\nu$, i.e., in resolution, at higher l/d . The Doppler widths are better in the case without scattering compared to those with it, more for higher h/d ,

but only at a low enough l/h, when they become independent of l/d. On the contrary, at high enough l/h, Doppler widths are almost independent of h/d and of the presence or absence of scattering from collimator walls.

Table

Total Ψ and local $\mathcal{P}$ flux of atoms, total θ and local χ number of atoms (30, 38), Doppler width $\Delta\nu$ (16) with ($\mathcal{R} \neq 0$) and without ($\mathcal{R} = 0$) atomic scattering from collimator walls, for two collimators with different sets of d, h, l parameters, called in ref. /4/ "low" and "high" collimation, $\delta = 1$ mm, $2\tau = 6$ mm.

Collimation	d	h mm	l	$\mathcal{R}$	Ψ, s^{-1}	$\mathcal{P}$, s^{-1}	θ	χ	$\Delta\nu$, MHz
low	1	1	113	$\neq 0$	1.108×10^{11}	3.326×10^{7}	4.345×10^{5}	9.262×10^{1}	22.35
				$=0$	4.755×10^{10}	3.281×10^{7}	1.463×10^{5}	9.137×10^{1}	22.35
high	0.7	7	117	$\neq 0$	8.165×10^{9}	1.526×10^{7}	2.922×10^{4}	4.248×10^{1}	20.67
				$=0$	3.597×10^{8}	1.350×10^{7}	1.003×10^{3}	3.759×10^{1}	20.67

Calculation performed for "standard" values of (1) $n_s = 4 \times 10^{15}$ atom/m^3 and (2) $v_s = 250$ m/s. At any n and v, the values of Ψ and $\mathcal{P}$ are obtained from those of the table multiplying them by $nv/n_s v_s$: see (14, 28), of θ and χ multiplying by n/n_s : see (14, 28), of $\Delta\nu$ multiplying by v/v_s : see (16).

Next we give in the table all integral fluxes Ψ and $\mathcal{P}$, numbers of atoms θ and χ (21, 22), and Doppler widths $\Delta\nu$ (16), for two collimators used in the real experiments of ref. /4/. One sees the better collimation efficiency $\mathcal{P}/\Psi$ or χ/θ and its higher improvement without scattering for the second collimator, but the almost unchanged Doppler width $\Delta\nu$ in all cases.

To illustrate the rapid change of, e.g., Ψ with T, we present a calculation in fig. 6, according to the procedure explained in the caption to the table, with the experimental correction, discussed in the next passage, included.

Further we discuss an experiment to check our calculations with respect to possible errors in the empirical data about $P(T)$ and/or effective temperature located at another place than the measured one T with a sample of pure $_{63}Eu$ /4/. The total number of evaporated atoms has been obtained experimentally by weight measurements before and after oven heating and theoretically by integrating

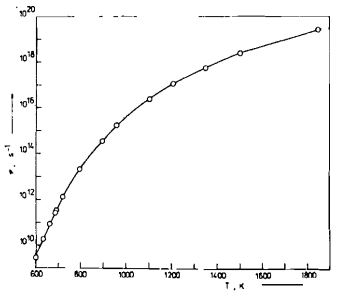

Fig. 6. Dependence of total flux Ψ (for one of both stable isotopes) of pure natural $_{63}Eu$ on oven sample temperature T (high collimation, with scattering $\mathcal{R} \neq 0$).

the total flux Ψ over time. A ratio 1.689 was obtained, which corresponds to a temperature higher by 12.5 K. A corresponding correction has to be introduced in all flux and number predictions.

6. Generalizations beyond basic assumptions

The first assumption of section 1, about vapour in the oven being saturated, can be checked and its violation taken into account experimentally. The way to do it has been shown elsewhere, especially by our quantity $c_i(t)$ (6) of ref. /4/, giving the ratio of the real to saturated vapour concentration (for $\theta = \chi$ in the notations of that reference) and by the change:

$$n \longrightarrow n' = c_i(t)\, n. \tag{25}$$

The second assumption of a high mean free path $\lambda \gg h$ is actually valid for low vapour pressures $P \lesssim 10^{-3}$ Torr, which is the case in real situations /4/. However, if its violation might happen, one can treat the case approximately by the following changes:

$$\begin{aligned} h &\longrightarrow h' = h\sqrt{\lambda/(\lambda+h)} \\ l &\longrightarrow l', \quad l'-h' = l-h \\ n &\longrightarrow n' = n\sqrt{\lambda/(\lambda+h)} \end{aligned} \tag{26}$$

The third assumption of diffuse scattering without reflection $\mu \approx 1$ has been done in other publications /6/, and is justified by the coincidence of the present theory with the experiment of ref. /7/ for angular distribution widths, discussed at the end of section 2. However if it is violated, one can treat the case approximately by the following changes:

$$\begin{aligned} h &\longrightarrow h' = h\mu \\ l &\longrightarrow l', \quad l'-h' = l-h \\ n &\longrightarrow n' = n \end{aligned} \tag{27}$$

In particular, the case of reflection without scattering $\mu = 0$ would be equivalent to disappearance of the collimator (it becomes like a part of the oven): $h \longrightarrow h' = 0$, $1 \longrightarrow 1' = 1 - h$.

Appendix

We introduce the following notations in addition to (5, 6, 9-14, 18):

$$\gamma_o = \frac{1}{2\sqrt{\pi}}\, n v \sigma \quad , \qquad \theta_o = \frac{\pi}{8}\, n \delta \sigma \tag{28}$$

and

$$F(\bar{\ell}_\tau)\, \hat{\varkappa}\, G(\bar{\ell}_\tau) = F(\ell) G(\ell) \quad , \qquad \bar{\varkappa} = \varkappa \times \min\left[1,\ 3/(2\varepsilon)\right] . \tag{29}$$

By integrating (21) to get γ , θ in two dimensions, we obtain directly:

$$\gamma = \gamma_o \left\{ (1-\varkappa_o)\left[1 - \frac{g(d/h)}{d/h}\right] + \varkappa_o \frac{g(h/d)}{h/d} \right\}$$

$$\theta = \theta_o \left\{ 1 - (1-\varkappa_o)\, \frac{\ell n\left[\sqrt{f(d/h)} + d/h\right]}{d/h} - \varkappa_o \frac{1}{\sqrt{f(d/h)} + d/h} \right\} . \tag{30}$$

By integrating (22) to get γ , χ in a one-dimensional approximation along the laser ray, valid in the case $\delta \ll 2\varrho$, we obtain:

$$\gamma_o^{\tau} = \sum_{i=1}^{4} \gamma_{i-1}^{i} \quad , \qquad \chi_o^{\tau} = \sum_{i=1}^{4} \chi_{i-1}^{i} . \tag{31}$$

The various terms are written as follows:

$$\gamma_{\tau_o}^{\tau_1} = \frac{1}{2}\, \eta_o^{(S)} S_1 \left\{ a_{\tau_o}^{\tau_1} \left[\frac{g(\tau_1/\bar{\ell}_{\tau_1})}{\tau_1/\bar{\ell}_{\tau_1}} + \frac{1}{f(\tau_1/\bar{\ell}_{\tau_1})} \right] \right.$$

$$\left. + b_{\tau_o}^{\tau_1} \left[\frac{1}{f(\tau_{1-}/\bar{\ell}_{\tau_1})} - \frac{1}{f(\tau_{1+}/\bar{\ell}_{\tau_1})} \right] \right\} \tag{32}$$

$$\chi_{\tau_o}^{\tau_1} = \eta_o^{(V)} V_1 \left\{ a_{\tau_o}^{\tau_1} \frac{1}{\sqrt{f(\tau_1/\bar{\ell}_{\tau_1})}} + b_{\tau_o}^{\tau_1} \left[\frac{1}{\sqrt{f(\tau_{1-}/\bar{\ell}_{\tau_1})}} - \frac{1}{\sqrt{f(\tau_{1+}/\bar{\ell}_{\tau_1})}} \right] \right\}$$

with

$$a_{\tau_o}^{\tau_1} = \hat{\varkappa} + \varkappa d/\varrho_+ \qquad b_{\tau_o}^{\tau_1} = \varkappa\, \bar{\ell}_{\tau_o} \bar{\ell}_{\tau_1} / (\varrho_+ \tau_1) \tag{33}$$

further

$$\gamma_{\tau_1}^{\tau_2} = \frac{1}{2}\, \eta_o^{(S)} S_2 \left\{ a_{\tau_1}^{\tau_2} \left[g(\bar{\tau}_2/\bar{\ell}_{\tau_2}) - g(\bar{\tau}_1/\bar{\ell}_{\tau_1}) + \frac{\bar{\tau}_2/\bar{\ell}_{\tau_2}}{f(\bar{\tau}_2/\bar{\ell}_{\tau_2})} - \frac{\bar{\tau}_1/\bar{\ell}_{\tau_1}}{f(\bar{\tau}_1/\bar{\ell}_{\tau_1})} \right] \right.$$

$$\left. - b_{\tau_1}^{\tau_2} \left[\frac{1}{f(\bar{\tau}_1/\bar{\ell}_{\tau_1})} - \frac{1}{f(\bar{\tau}_2/\bar{\ell}_{\tau_2})} \right] + c_{\tau_1}^{\tau_2} \left[\frac{1}{f(\tau_{1+}/\bar{\ell}_{\tau_1})} - \frac{1}{f(\tau_{2+}/\bar{\ell}_{\tau_2})} \right] \right\}$$

$$\chi_{\tau_1}^{\tau_2} = \eta_o^{(V)} V_2 \left\{ a_{\tau_1}^{\tau_2} \left[\frac{\bar{\tau}_2/\bar{\ell}_{\tau_2}}{\sqrt{f(\bar{\tau}_2/\bar{\ell}_{\tau_2})}} - \frac{\bar{\tau}_1/\bar{\ell}_{\tau_1}}{\sqrt{f(\bar{\tau}_1/\bar{\ell}_{\tau_1})}} \right] \right. \tag{34}$$

$$\left. - b_{\tau_1}^{\tau_2} \left[\frac{1}{\sqrt{f(\bar{\tau}_1/\bar{\ell}_{\tau_1})}} - \frac{1}{\sqrt{f(\bar{\tau}_2/\bar{\ell}_{\tau_2})}} \right] + c_{\tau_1}^{\tau_2} \left[\frac{1}{\sqrt{f(\tau_{1+}/\bar{\ell}_{\tau_1}}} - \frac{1}{\sqrt{f(\tau_{2+}/\bar{\ell}_{\tau_2})}} \right] \right\}$$

with

$$a_{\tau_1}^{\tau_2} = \frac{\varrho_+ \varrho_-}{\varrho^2 \tau_2} \bar{\ell}_{\tau_2} \left[\hat{\varkappa} + \varkappa d (\varrho + d/4)/\varrho_+^2 \right]$$

$$b_{\tau_1}^{\tau_2} = \frac{\varrho_- \bar{\ell}_{\tau_1} \bar{\ell}_{\tau_2}}{\varrho^2 \tau_2} \left[\hat{\varkappa} + \varkappa d_-/\varrho_+ \right] \qquad c_{\tau_1}^{\tau_2} = \varkappa\, \bar{\ell}_{\tau_1} \bar{\ell}_{\tau_2} / (\varrho_+ \tau_2) \tag{35}$$

and for $i = 3, 4$

$$\gamma_{\tau_{i-1}}^{\tau_i} = \frac{1}{2}\, \eta_o^{(S)} S_2 \left\{ a_{\tau_{i-1}}^{\tau_i} \left[\ell n \left(\frac{\tau_{i+}\, \bar{\ell}_{\tau_{i-1}}}{\tau_{i-1+}\, \bar{\ell}_{\tau_i}} \right) \frac{f\left(\frac{\tau_{i-1+}}{\bar{\ell}_{\tau_{i-1}}}\right)}{f\left(\frac{\tau_{i+}}{\bar{\ell}_{\tau_i}}\right)} - \frac{1}{f\left(\frac{\tau_{i-1+}}{\bar{\ell}_{\tau_{i-1}}}\right)} - \frac{1}{f\left(\frac{\tau_{i+}}{\bar{\ell}_{\tau_i}}\right)} \right] \right.$$

$$+\frac{3}{2}\,b^{\tau_i}_{\tau_{i-1}}\left[\frac{f\left(\frac{\tau_{i-1+}}{\bar\ell_{\tau_{i-1}}}\right)-\frac{1}{3}}{f\left(\frac{\tau_{i-1+}}{\bar\ell_{\tau_{i-1}}}\right)}-\frac{\tau_{i-1+}}{\tau_{i+}}\,\frac{\bar\ell_{\tau_i}}{\bar\ell_{\tau_{i-1}}}\,\frac{f\left(\frac{\tau_{i+}}{\bar\ell_{\tau_i}}\right)-\frac{1}{3}}{f\left(\frac{\tau_{i+}}{\bar\ell_{\tau_i}}\right)}\right.$$

$$\left.-\frac{\tau_{i-1+}}{\bar\ell_{\tau_{i-1}}}\left(g\left(\frac{\tau_{i+}}{\bar\ell_{\tau_i}}\right)-g\left(\frac{\tau_{i-1+}}{\bar\ell_{\tau_{i-1}}}\right)\right)\right]\Bigg\} \qquad (36)$$

$$\chi^{\tau_i}_{\tau_{i-1}}=\eta_o^{(V)}V_2\left\{a^{\tau_i}_{\tau_{i-1}}\left[\ell n\left(\frac{\tau_{i+}}{\tau_{i-1+}}\,\frac{\bar\ell_{\tau_{i-1}}}{\bar\ell_{\tau_i}}\right)\frac{1+\sqrt{f\left(\frac{\tau_{i-1+}}{\bar\ell_{\tau_{i-1}}}\right)}}{1+\sqrt{f\left(\frac{\tau_{i+}}{\bar\ell_{\tau_i}}\right)}}-\frac{1}{\sqrt{f\left(\frac{\tau_{i-1+}}{\bar\ell_{\tau_{i-1}}}\right)}}-\frac{1}{\sqrt{f\left(\frac{\tau_{i+}}{\bar\ell_{\tau_i}}\right)}}\right]\right.$$

$$\left.+\,b^{\tau_i}_{\tau_{i-1}}\left[\frac{f\left(\frac{\tau_{i-1+}}{\bar\ell_{\tau_{i-1}}}\right)-\frac{1}{2}}{\sqrt{f\left(\frac{\tau_{i-1+}}{\bar\ell_{\tau_{i-1}}}\right)}}-\frac{f\left(\frac{\tau_{i+}}{\bar\ell_{\tau_i}}\right)-\frac{1}{2}}{\sqrt{f\left(\frac{\tau_{i+}}{\bar\ell_{\tau_i}}\right)}}\right]\right\}$$

with

$$a^{\tau_i}_{\tau_{i-1}}=\varkappa\varepsilon\,\frac{\varrho_-}{\varrho}\begin{cases}1\\ \dfrac{\ell n(\tau_+/\tau_{3+})}{\ell n(\tau_-/\tau_{3-})}\end{cases}\qquad b^{\tau_i}_{\tau_{i-1}}=\varkappa\varepsilon\,\frac{\varrho_-}{\varrho}\,\frac{d}{\tau_{i-1+}}\begin{cases}1\,, & i=3\\ \dfrac{\tau_-}{\tau_+}\,, & i=4\end{cases} \qquad (37)$$

A two dimensional factorization approximation for φ , χ to take laser ray thickness in the case $2\varrho \lesssim \delta$ into account can be achieved easily as follows:

$$\varphi=\varphi_o^{\tau}\varphi_o^{\delta/2}/[S_o\eta^{(S)}(0)]$$
$$\chi=\chi_o^{\tau}\chi_o^{\delta/2}/[V_o\eta^{(V)}(0)]\,. \qquad (38)$$

To obtain $\Delta\nu$ (16), we have to find the solution u of (23):

$0\le u\le v_o$: $\quad u=\frac{1}{2}\,\frac{\alpha}{\beta}\,v_o$

$\alpha=1+\bar\varkappa(1-\varepsilon^{-1})\,,\quad \beta=1-\frac{\bar\varkappa}{2}(1+\varepsilon^{-1})$

$v_o\le u\le w_o$: $\quad u=\left[\alpha\gamma\left(\sqrt{1+\frac{\beta}{\alpha\gamma^2}}+1\right)-\beta\right]v_o$

$\alpha=\frac{3}{2}\,\varkappa/[1+\bar\varkappa(1-\varepsilon^{-1})]\,,\quad \beta=\varepsilon-1\,,\quad \gamma=1$

$v_o,\ w_o\le u$: $\quad u$ the same

$\alpha=\varkappa/[1+\bar\varkappa(1-\varepsilon^{-1})]\,,\quad \beta=\varepsilon-1\,,\quad \gamma=1+\beta/(2\alpha)\,.$

Then we find the limit t :

$d/3\le\tau+d/3\le\varrho$: $\quad t=\tau_+/\ell$

$\varrho<\tau+d/3\le 5d/2$: $\quad t=(\tau_++d/3)/[\frac{3}{2}(\ell-h)]$

$\varrho,\ 5d/2<\tau+d/3$: $\quad t=(\tau_-+d/3)/(\ell-h)\,.$

Both u (39) and t (40) are to be inserted in (24) to get u_o , and u_o into (16) to obtain $\Delta\nu$.

References

1. Otten E.W. Nucl.Phys., 1981, A354, p.471c.
2. Otten E.W. In: International School-Seminar on Heavy Ion Physics (Alushta). JINR, D7-83-644, Dubna, 1983, p.158.
3. Гангрский Ю.П., Маринова К.П., Марков Б.Н., Наджаков Е.Г., Оганесян Ю.Ц., Хан Ген И, Чан Конг Там. Изв.АН СССР сер. физ., 1985, 49, с.2261.

4. Gangrsky Yu.P., Han Gyong I, Marinova K.P., Markov B.N., Nadjakov E.G., Tran Cong Tam. JINR, E6-86-233, Dubna, 1986, submitted to Nucl.Instr.Meth. A.
5. Nadjakov E.G. JINR, E6-86-232, Dubna, 1986; submitted to J.Phys. E Sci.Instr.
6. Троицкий В.С. ЖТФ, 1962, 32, с.488.
7. Алхазов Г.Д., Барзах А.Е., Берлович Э.Е., Денисов В.П., Дернятин А.Г., Иванов В.С., Жерихин А.Н., Компанец О.Н., Летохов В.С., Мишин В.И., Федосеев В.Н. ЛИЯФ АН СССР, 908, Ленинград, 1983.
8. Несмеянов А.Н. Давление пара химических элементов. Изд. АН СССР, Москва, 1961.

Received by Publishing Department
on April 14, 1986.

Наджаков Е.Г. E6-86-231
Коллимация атомного пучка

Старая проблема коллимации атомного пучка рассмотрена заново в связи с развитием лазерной спектроскопии в ядерной физике. Найдены распределения атомного потока и плотности в пространстве и по скорости при использовании эмпирических данных относительно зависимости давления пара от температуры, максвелловского распределения скоростей в тигле и эмпирически обоснованной гипотезы относительно рассеяния атомов от стенок коллиматора, определяющей трансмиссию коллиматора. В результате найдены интегральные потоки и числа атомов, покидающих тигель через область взаимодействия атомного пучка - лазерного луча - флуоресцентного света, а также во всех направлениях, следующая отсюда эффективность коллимации, как и Допплеровская ширина линии. Они предназначены для использования в другой публикации, посвященной определению и предсказанию параметров лазерного спектрометра.

Работа выполнена в Лаборатории ядерных реакций ОИЯИ.

Препринт Объединенного института ядерных исследований. Дубна 1986

Nadjakov E.G. E6-86-231
Atomic Beam Collimation

The old problem of atomic beam collimation is considered once more in connection with the development of laser spectroscopy in nuclear physics. The distributions of the atomic flux and density over space and velocity are found by using empirical data about vapour pressure dependence on temperature, the Maxwell velocity distribution in oven, and an empirically based hypothesis about atom scattering from collimator walls determining the collimator transmission. Consequently, the integral fluxes and numbers of atoms leaving the oven through the atomic beam - laser ray - fluorescence light interaction region and also in all directions, the consequent collimation efficiency, as well as the Doppler line width are found. They are to be used in another publication concerning determination and prognosis of laser spectrometer parameters.

The investigation has been performed at the Laboratory of Nuclear Reactions, JINR.

Preprint of the Joint Institute for Nuclear Research. Dubna 1986